https://doi.org/10.3311/PPci.20424

Periodica Polytechnica Civil Engineering, 66(4), pp. 1023–1031, 2022

Numerical Simulation of 3-D Internal Crack Propagation in Rock under Semi-circle Bending

Zhitao Zhang[1*], Weijie Gu[2]

[1] Geotechnical Engineering Department, Nanjing Hydraulic Research Institute, Nanjing 210019, China
[2] Shandong Yellow River Reconnaissance Design and Research Institute Co., Ltd, Jinan 250013, China
[*] Corresponding author, e-mail: ztzhang@nhri.cn

Received: 09 May 2022, Accepted: 21 June 2022, Published online: 29 June 2022

Abstract

Semi-circle bending (SCB) test is an important test in the field of rock fracture. In order to investigate the propagation process of 3-D internal cracks under semi-circular bending, numerical simulations of SCB specimens were carried out based on the finite element method and adaptive mesh technique. The results show that the numerical simulation results of this method are in good agreement with the previous laboratory test. The symmetrical loading model belongs to the pure I loading where the value of K_I is positively related to the bottom load span *S*/*R*. The asymmetric loading model belongs to mix-mode loading. With the increase of unilateral load span *S*2/*R*, there is a decline and then a rise of the value of SIF at the same point at the crack tip. The *S*2/*R* is an important factor affecting the mechanical properties of rock specimens. The crack propagation path was obtained based on the maximum tensile stress (MTS) criterion. In-plane propagation of the internal crack in the symmetrically loading model leads to failure of the specimen. Wing propagation of the internal crack in the asymmetrically loading model causes the specimen to fracture into two asymmetrical parts. Quantitative analysis of the internal crack propagation of the symmetrical loading model shows that the growth rate of the lower end of the crack is the largest, and the upper end of the crack is the smallest. The above results can provide a reference for the research on the propagation of 3-D internal cracks of SCB specimens.

Keywords

rock fracture, semi-circular bending, propagation path, fracture characteristics, 3-D crack

1 Introduction

Semi-circular bend (SCB) specimens are widely used in the study of fracture behavior of brittle materials such as rocks due to their simple geometry, manufacturing process, and test operations [1]. The SCB specimen was first proposed by Chong and Kuruppu [2] and Chong et al. [3] to determine the fracture parameter KIC. Further, some scholars changed the initial position of the prefabricated crack of the specimen, so that the SCB specimen has the ability to determine the fracture parameters in the mixed mode [4–7].

Since the SCB specimen was proposed, many scholars have carried out a lot of research on the laboratory test and numerical research. In recent years, in the field of laboratory tests, Aliha et al. [8–9] conducted SCB tests on the PMMA panels by controlling the specimen geometry and loading parameters, and used the SCB specimens to carry out the research on the mixed fracture toughness characteristics of asphalt mixtures. Huang et al. [10] explored the flexural properties of asphalt mixtures with notched SCB specimens. Zhao et al. [11] carried out research on the tensile properties and fracture properties of coal by SCB test. Jiang et al. [12] used gypsum 3D printing materials to carry out SCB tests, and the test results were consistent with the fracture paths of rocks. Feng et al. [13] used SCB test to study the effect of temperature on the mode-I fracture toughness and fracture characteristics of sandstone. Wang et al. [14] conducted laboratory experiments on the interaction between natural fractures and hydraulic fractures using SCB specimens. Fu et al. [15] studied the effects of interaction between concrete-gypsum interface and edge crack on the failure behavior of the specimens in semicircular bend (SCB) test. Further, Fu et al. [16] carried out the notched NBD tests and the SCB tests. The results show that the fracture toughness of rocks' specimens obtained by NBD tests was higher than that of the SCB tests.

Cite this article as: Zhang, Z., Gu, W. "Numerical Simulation of 3-D Internal Crack Propagation in Rock under Semi-circle Bending", Periodica Polytechnica Civil Engineering, 66(4), pp. 1023–1031, 2022. https://doi.org/10.3311/PPci.20424

In the field of theoretical and numerical research, Lim et al. [17] proposed the calculation method of stress intensity factor (SIF) for notched SCB specimens in 1993, which provided a means for the study of fracture parameters in mixed mode. Zhao et al. [18] used the discrete element model to numerically simulate the dynamic fracture toughness of the SCB specimen with bottom groove. Eftekhari et al. [19] discussed the fracture properties of notched SCB specimens under mixed mode loading using the extended finite element method. Fayed [20] used a finite element program to evaluate the mode I/II SIF of SCB specimens of quasi-brittle materials with edge cracks. In recent years, Haeri et al. [21–22] carried out numerical simulations of edge notched disk (END) and hollow center cracked disc (HCCD) in Brazilian test, taking into account the effect of particle size on tensile fracture toughness. It should be pointed out that the above numerical simulation methods also have the potential ability to simulate SCB tests.

Current research is mostly limited to surface and penetrating cracks, whether in laboratory tests or numerical research. However, the 3-D internal cracks in the rock have a great influence on its fracture failure performance. In the field of fracture mechanics, the arbitrary propagation of 3-D internal cracks has difficulties in modeling and mesh processing [23]. In view of the above problems, based on the finite element method, this paper adopts the adaptive mesh technique to establish the SCB model with symmetrical loading and the SCB model with asymmetric loading. Based on M-integral, the SIF distribution of I, II and III at the crack front is given. Numerical research is carried out on the fracture mode, propagation path, failure pattern and propagation rate of the SCB model, which provides a numerical basis for 3-D internal crack propagation path simulation and fracture characteristics research.

2 Numerical methods and models

Numerical simulation method is an effective means to analyze the fracture process of rocks containing internal cracks. In terms of the accuracy of the SIF values, the interaction integration method is the most accurate method for extracting mixed-mode of SIF [24]. Combining the M-integration method with the adaptive mesh technique can better solve the problem of the calculation accuracy of the SIF values at the crack front and the grid processing. Therefore, in this paper, the above method is used to simulate the fracture process of the SCB model containing 3-D internal cracks.

2.1 Numerical models

In this paper, two sets of SCB models with three-dimensional internal cracks are established, as shown in Fig. 1. The model is semicircular with a radius R of 50 mm and a thickness t of 50 mm. The shape of the internal crack is circular, and the diameter a is 10 mm. The internal crack depth h was 15 mm. In the Fig. 1, 2S is the bottom loading span, and S1 and S2 are the left and right loading spans, respectively.

The research plan is shown in Table 1. In the symmetrical loading model, the values of a/R and t/R are fixed, and the effect of S/R changes on the fracture characteristics of the SCB model containing 3-D internal cracks is explored. Correspondingly, in the asymmetric loading model, the values of a/R, t/R, and S1/R are fixed to explore the effect of changes in $S2/R$. It should be noted that in order to verify the accuracy of this numerical simulation method in simulating the crack propagation path, two numerical models are established, and the above models are not included in the research plan.

Fig. 2 shows the mesh properties of internal cracks in the SCB model. The Cartesian coordinate system X-Y represents the long axis and short axis directions of the elliptical crack surface, respectively. In Fig. 2(a), the length of one rotation along the long axis A point counterclockwise

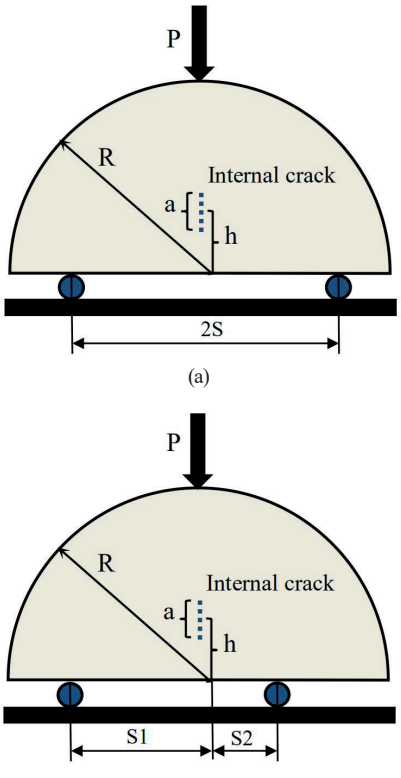

Fig. 1 The Schematic Diagram of the SCB Model; (a) the symmetric loading model, (b) the asymmetric loading model

Table 1 Research plan

Model type	Model Number	R (mm)	a (mm)	t (mm)	a/R	S/R	$2S$ (mm)	$S2/R$	$S1$ (mm)	$S2$ (mm)
Symmetric loading (Group-A)	A-1	50	10	50	0.2	0.5	50	/	/	/
	A-2	50	10	50	0.2	0.6	60	/	/	/
	A-3	50	10	50	0.2	0.7	70	/	/	/
	A-4	50	10	50	0.2	0.8	80	/	/	/
Asymmetric loading (Group-B)	B-1	50	10	50	0.2	/	/	0.1	25	5
	B-2	50	10	50	0.2	/	/	0.2	25	10
	B-3	50	10	50	0.2	/	/	0.3	25	15
	B-4	50	10	50	0.2	/	/	0.4	25	20
	B-5	50	10	50	0.2	/		0.5	25	25
	B-6	50	10	50	0.2	/		0.6	25	30
	B-7	50	10	50	0.2	/		0.7	25	35
	B-8	50	10	50	0.2	/		0.8	25	40

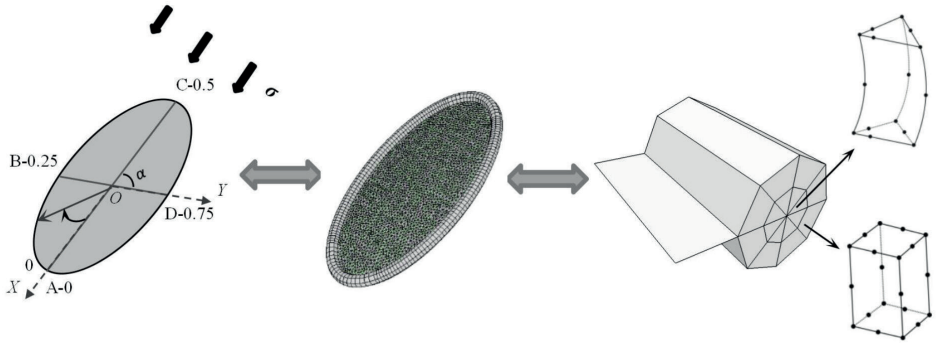

Fig. 2 Crack Surface Coordinate System and Mesh Properties; (a) the schematic diagram of the crack surface, (b) the mesh pattern of crack surface, (c) The form of elements

is defined as 1. The singular elements are implanted at the crack fronts and a symmetric mesh is used to reduce the local discrete error. The actual crack surface mesh pattern is shown in Fig. 2(b). Conservative integration evaluation is performed on two element rings around the crack front. The inner ring of a 15-node singular wedge element and the outer ring of a 20-node hexahedral element are shown in Fig. 2(c).

In this study, the model is set to isotropic elasticity, where elastic modulus E = 17.92 Gpa, Poisson's ratio v = 0.192, density ρ = 2.3 g/cm^3. A stress boundary in the Y-direction is applied to the upper part of the model, while a fixed displacement constraint in the Y-direction is applied to the bottom of the model.

2.2 Calculation principle of SIF and T-stress

M-integration is used to calculate the value of SIF. The J-integration [25] of the superposition of two equilibrium states can be assumed as:

$$\bar{J} = \int_{\Gamma}\left[\left(\sigma_{ij}^{(1)}+\sigma_{ij}^{(2)}\right)\frac{\partial u_i^{(1)}+\partial u_i^{(2)}}{\partial x}-\left(W^{(1)}+W^{(2)}\right)\delta_{1j}\right]\frac{\partial_q}{\partial_{xj}}ds, \tag{1}$$

$$= \bar{J}^{(1)}+\bar{J}^{(2)}+\bar{M}^{(1,2)}. \tag{2}$$

For linear elastic materials, the strain energy density $W = \sigma_{ij}\varepsilon_{ij}/2$. According to Betti's reciprocity theorem:

$$W^{(1,2)} = \sigma_{ij}{}^{(1)}\varepsilon_{ij}{}^{(2)} = \sigma_{ij}{}^{(2)}\varepsilon_{ij}{}^{(1)}. \tag{3}$$

The parameters in Eq. (2) can be expressed as:

$$\bar{J}^{(1)} = \int_{\Gamma}\left[\sigma_{ij}^{(1)}\frac{\partial u_i^{(1)}}{\partial x_1}-W^{(1)}\delta_{1j}\right]\frac{\partial_q}{\partial_{xj}}ds, \tag{4}$$

$$\bar{J}^{(2)} = \int_{\Gamma}\left[\sigma_{ij}^{(2)}\frac{\partial u_i^{(2)}}{\partial x_1}-W^{(2)}\delta_{1j}\right]\frac{\partial_q}{\partial_{xj}}ds, \tag{5}$$

$$\bar{M}^{(1,2)} = \int_{\Gamma}\left[\begin{array}{l}\sigma_{ij}^{(1)}\dfrac{\partial u_i^{(2)}}{\partial x_1}+\sigma_{ij}^{(2)}\dfrac{\partial u_i^{(1)}}{\partial x_1}\\ -\dfrac{1}{2}\left(\sigma_{ij}{}^{(1)}\varepsilon_{ij}{}^{(2)}+\sigma_{ij}{}^{(2)}\varepsilon_{ij}{}^{(1)}\right)\delta_{1j}\end{array}\right]\frac{\partial_q}{\partial_{xj}}ds. \tag{6}$$

The relationship between the energy release rate G and the stress intensity factor K in the two equilibrium states is as follows:

$$G = J = \frac{1-\nu^2}{E}\left(K_I^{(1)} + K_I^{(2)}\right)^2 + \frac{1-\nu^2}{E}\left(K_{II}^{(1)} + K_{II}^{(2)}\right)^2 + \frac{1+\nu}{E}\left(K_{III}^{(1)} + K_{III}^{(2)}\right)^2, \quad (7)$$

$$J^{(1)} = \frac{1-\nu^2}{E}\left(K_I^{(1)}\right)^2 + \frac{1-\nu^2}{E}\left(K_{II}^{(1)}\right)^2 + \frac{1+\nu}{E}\left(K_{III}^{(1)}\right)^2, \quad (8)$$

$$J^{(2)} = \frac{1-\nu^2}{E}\left(K_I^{(2)}\right)^2 + \frac{1-\nu^2}{E}\left(K_{II}^{(2)}\right)^2 + \frac{1+\nu}{E}\left(K_{III}^{(2)}\right)^2, \quad (9)$$

$$M^{(1,2)} = 2\left[\frac{1-\nu^2}{E}K_I^{(1)}K_I^{(2)} + \frac{1-\nu^2}{E}K_{II}^{(1)}K_{II}^{(2)} + \frac{1+\nu}{E}K_{III}^{(1)}K_{III}^{(2)}\right]. \quad (10)$$

By choosing a specific auxiliary field, the solution of the SIF of K_I, K_{II} and K_{III} at the crack front can be obtained by using the interactive M-integration of the far field, as follows:

$$M^{(1,2)} = 2\frac{1-\nu^2}{E}K_I, \quad (11)$$

$$K_I = \frac{E}{2(1-\nu^2)}M^{(1,2)} = \frac{E}{2(1-\nu^2)}\bar{M}^{(1,2)}, \quad (12)$$

$$K_{II} = \frac{E}{2(1-\nu^2)}M^{(1,2)} = \frac{E}{2(1-\nu^2)}\bar{M}^{(1,2)}, \quad (13)$$

$$K_{III} = \frac{E}{2(1+\nu)}M^{(1,2)} = \frac{E}{2(1+\nu)}\bar{M}^{(1,2)}. \quad (14)$$

In the above equation, Γ is the integral curve away from the front edge of the crack front. δ_{ij} is the Clodic symbol. q is the smooth function. $\sigma_{ij}^{(1)}$, $\varepsilon_{ij}^{(1)}$ and $u_i^{(1)}$ is the finite element solution.

In the series expansion of the linear elastic crack tip stress field in Williams [26], the second non-singular term is called the elastic T-stress and represents the stress acting parallel to the crack surface. In this study, the general method of T-stress solution is adopted [27, 28].

2.3 Validation of numerical methods

Before carrying out the numerical simulation of the SCB model, the validity of the simulation method is firstly verified. Two more conventional models are established, namely the model with horizontal internal crack under uniaxial tension [29] and the sandstone SCB model with bottom cuts [4] at different angles (β = 0°, β = 30°, β = 54°). The numerical simulation results and laboratory test results are shown in Fig. 3.

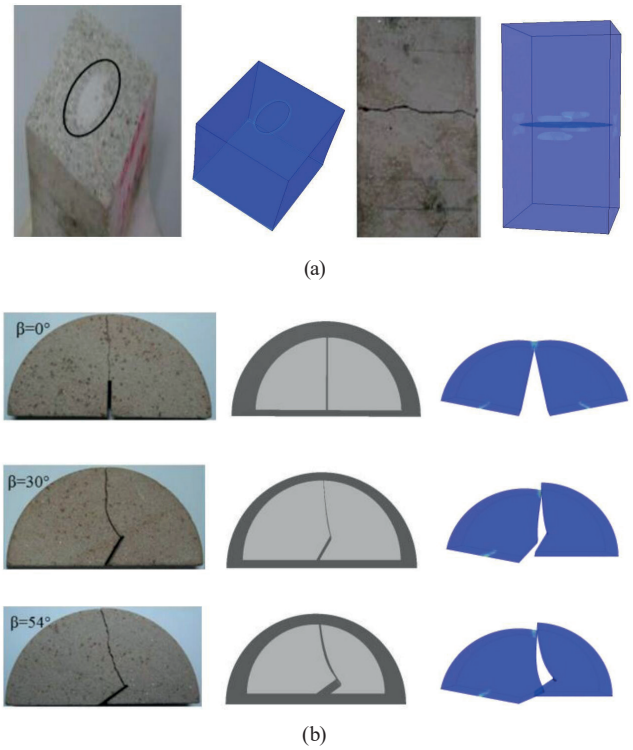

(a)

(b)

Fig. 3 Numerical simulation and laboratory test results; (a) comparison of numerical simulation results and literature [29], (b) comparison of numerical simulation results and literature [4]

It can be seen that the numerical method in this paper can simulate the whole process of 3-D internal crack from propagation to specimen fracture. At the same time, the simulation results are in good agreement with the laboratory test results.

3 Analysis of numerical calculation results

The SIF (K_I, K_{II} and K_{III}) for the three fracture modes can be calculated simultaneously using M-integration. The SIF describes the severity of the stress singularity near the crack tip. T-stress can significantly affect crack initiation and crack propagation path.

3.1 Symmetrically loading model

Fig. 4 shows the typical distribution of K_I and T-stress values in Group-A models. Considering that the models in Group-A belong to mode-I fracture, only the variation curve of the relative position of dimensionless KI along the crack front is shown in Fig. 4(a). The $K_n/|K_{n\max}|$ is defined as the dimensionless SIF, where n = I, II, III. Similarly, the variation curve of the relative position of the dimensionless T-stress along the crack front is shown in Fig. 4(b).

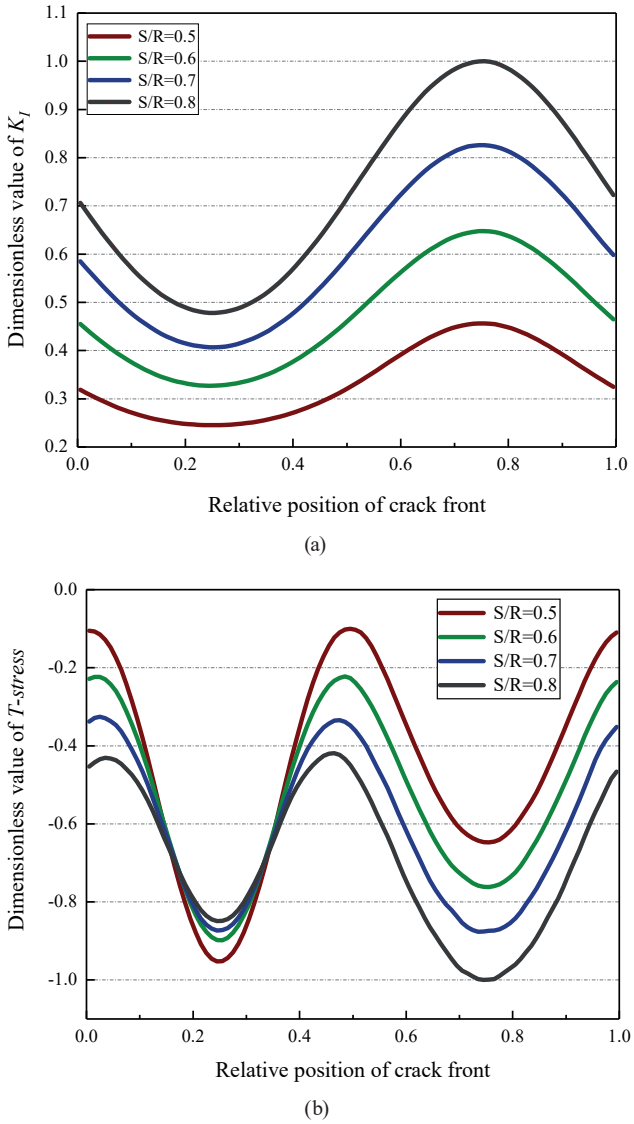

Fig. 4 The typical distribution of K_I and *T*-stress values of Group-A; (a) the dimensionless value of K_I, (b) the dimensionless value of *T*-stress

It can be seen from Fig. 4 as follows:

(1) Relative to the magnitude of K_I, the values of K_{II} and K_{III} are almost negligible to zero, which means that the crack surface is under great tension before crack initiation, so the crack is more inclined to expand along the original crack surface. This is consistent with the crack propagation along the plane in the subsequent crack propagation path simulation.

(2) The K_I at the lower end of the crack is the largest and the upper end is the smallest, indicating that the lower end of the crack is more prone to cracking and the extent of propagation is relatively greater.

(3) When *a*/*R* and *t*/*R* are fixed, K_I increases with the increase of *S*/*R*, which is the same as that of the SCB specimen with notches [19].

(4) Under the pure mode-I loading, the *T*-stress is always negative. In this mode, the crack propagation is stable, and the propagation direction is not deflected [30−31]. The variation of *T*-stress with *S*/*R* at the lower end of the crack front is more severe than that at the upper end of the crack.

3.2 Asymmetrically loading model

The variation of dimensionless SIF of Group-B is given as shown in Fig. 5.

It can be seen as follows:

(1) The SIF distribution of the B-4 and B-5 models is consistent with the symmetrical loading model, and the fracture mode is pure mode-I fracture. The numerical simulation method is not sensitive to the identification of asymmetric loading modes of small-scale eccentricity along the model center direction. The value of K_{II} and K_{III} were found in other models in group B, which were judged to be mixed-mode fracture.

(2) With the increase of *S*2/*R*, the value of K_I at one point on the crack front first decreases and then increases. Models B-1, B-2, and B-3 have the strongest mode-I effect at the upper end of the crack and the weakest at the lower end. The rest of the models are the opposite.

(3) With the increase of *S*2/*R*, the value of K_{II} first changed to 0, then increased gradually, and the direction of shear action changed. It should be noted that when the *S*2/*R* value is small, the mode-II effect is stronger. Models B-1, B-2, and B-3 have the strongest mode-II effect at the lower end of the crack, and models B-6, B-7, and B-8 have the opposite effect.

(4) Similar to the change trend of K_{II}, with the increase of *S*2/*R*, the value of K_{III} first changed to 0, and then gradually increased. In all models in this group, the value of K_{III} peaked at the relative positions of 0 and 0.5 along the crack front.

(5) The distribution of normalized *T*-stress is not given here. It should be noted that the discussion of *T*-stress in the current research is mostly based on the 2-D problem under the mode-I or mode-I/II loading. The effect of *T*-stress on the 3-D internal crack propagation mechanism is one of the problems to be solved in the subsequent numerical research.

3.3 Crack propagation path

Based on the calculated SIF value, the maximum tensile stress (MTS) criterion was used in this study to calculate the propagation direction of the crack tip. Further, the relative amount of each crack tip node expansion is calculated

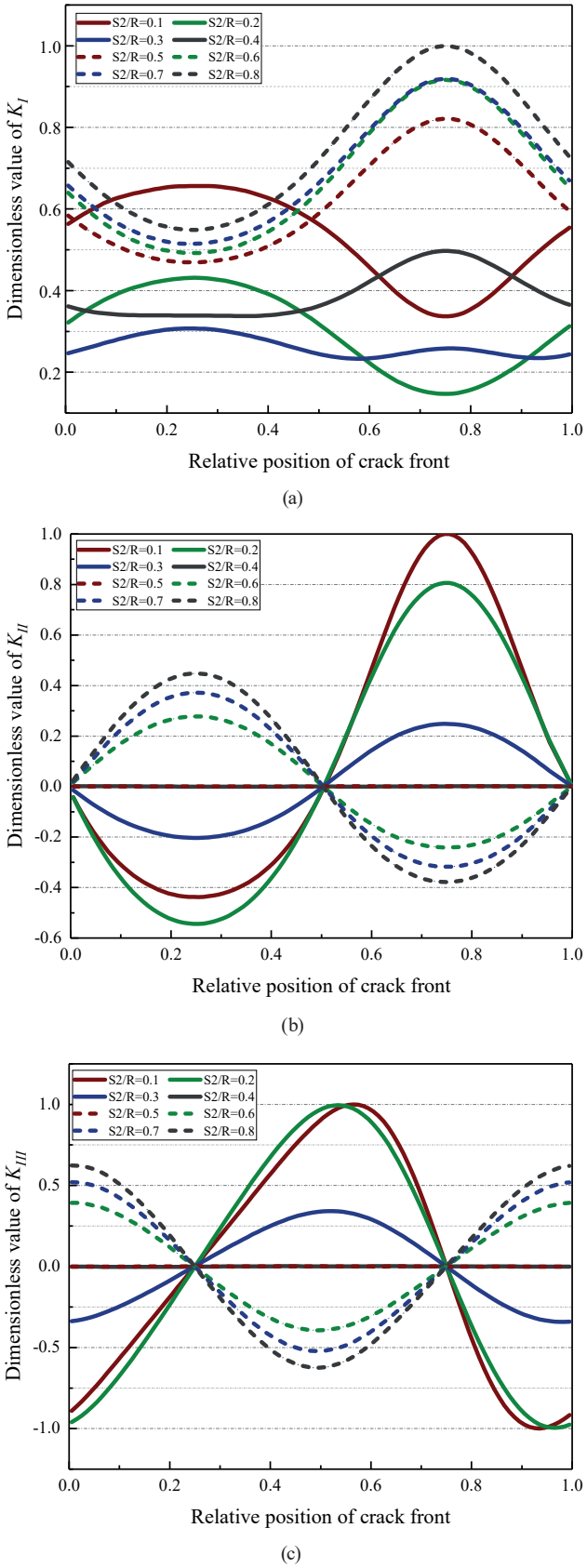

Fig. 5 The distribution of SIF of Group-B; (a) the dimensionless value of K_I, (b) the dimensionless value of K_{II}, (c) the dimensionless value of K_{III}

to obtain a new crack propagation surface. Fig. 6 shows the typical crack propagation paths and failure pattern in the two groups of models (models A-1, B-8).

Observing the fracture process of two specimens in Fig. 6, the following rules can be seen as follows:

(1) The internal crack of the A-1 model expands in plane under pure mode I loading. The lower end of the crack front reaches the bottom of the specimen first. Further, the crack spreads rapidly around, and finally a through crack is formed, which divides the specimen into two symmetrical parts. The ultimate failure mode of the specimen is pure mode I cracking.

(2) The internal crack of the B-8 model cracked under the mixed mode loading, and airfoil wrapping cracks appeared at the upper and lower tips of the crack. The positive and negative values of K_{II} determine the direction of shearing action, which further leads to opposite propagation directions of the upper and lower parts of the wing crack. The larger K_I value at the lower end of the crack causes the lower wing crack to reach the bottom of the model first. Further, the crack face expanded around, and finally a through crack is formed to broke the specimen into two asymmetrical parts. The ultimate failure mode of the specimen is mixed mode cracking. In Fig. 6(b), it can be observed that the fracture surface tends to slope towards the top of the model, which can be called the "correction effect" of shear stress. The purpose of the above action is to promote crack propagation in the plane perpendicular to the maximum principal tensile stress.

3.4 Crack growth rate

The propagation process of the crack initiation to the bottom of the specimen in the symmetrical loading model of Group-A was selected for quantitative analysis. Studies [32] have shown that the solution is more accurate when the median extension defaults to 15%~20% of the crack radius and the template radius defaults to 10% of the crack radius. In this section, the median extension is set to 15% of the crack radius, which is 0.75 mm. In order to obtain the growth length of each propagation step, the lower end (Point-A), upper end (Point-C), and right end (Point-D) of the crack are selected as characteristic points for quantitative analysis. The distribution of characteristic points with each propagation step is shown in Fig. 7.

It can be seen from Fig. 7 that the growth rate of the lower end of the crack (Point-A) is the largest, and the upper end of the crack (Point-C) is the smallest. Moreover, the growth rates of Point-A and Point-C tend to increase. How-

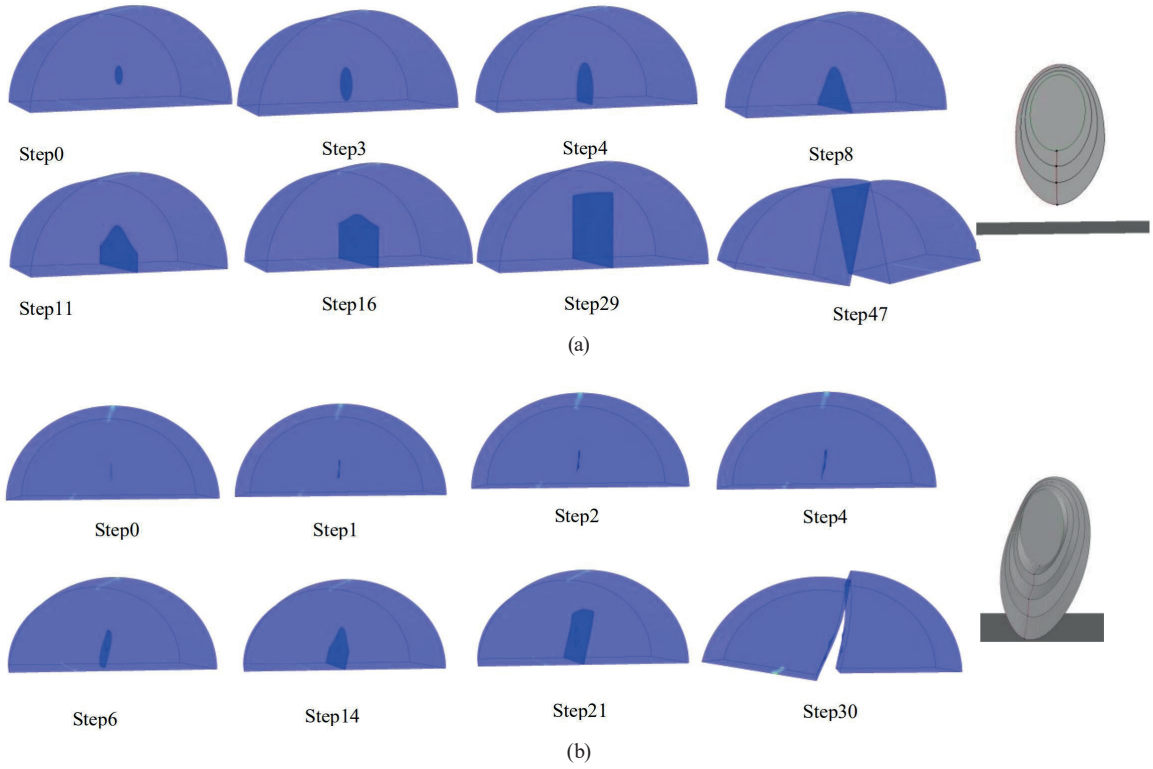

Fig. 6 The typical simulation results; (a) simulation results of model A-1, (b) simulation results of model B-8

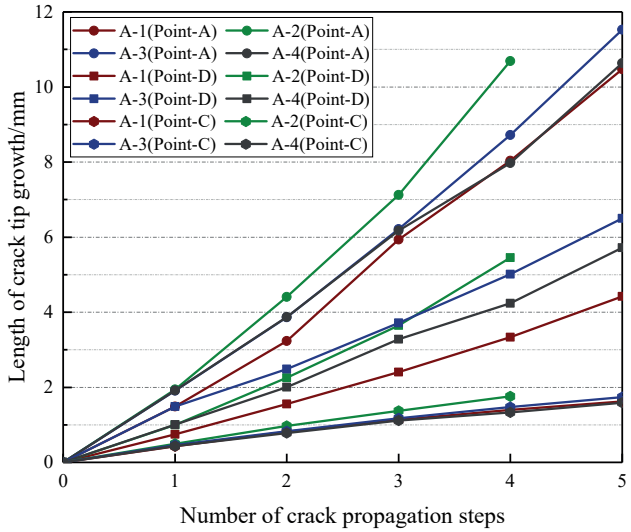

Fig. 7 the distribution of characteristic points with each propagation step

ever, the growth rate at Point-B remains almost unchanged. In addition, it can be seen that the internal crack of model A-2 has the fastest growth rate. After four propagation steps, the crack propagates to the bottom of the model.

4 Conclusions

In this paper, the internal crack propagation paths and fracture characteristics of SCB specimens under two loading modes are investigated. The main conclusions are as follows:

1. The numerical simulation results of this research method are in good agreement with the previous laboratory test results, and this method is an effective means to simulate 3-D crack propagation.

2. The symmetrical loading model belongs to the pure I loading where the value of K_I is positively related to the bottom load span S/R. The asymmetric loading model belongs to mix-mode loading. With the increase of unilateral load span $S2/R$, there is a decline and then a rise of the value of SIF at the same point at the crack tip.

3. In-plane propagation of the internal crack in the symmetrically loading model leads to failure of the specimen. Wing propagation of the internal crack in the asymmetrically loading model causes the specimen to fracture into two asymmetrical parts.

4. The quantitative analysis of the growth rate of the crack in the symmetrical loading model shows that the growth rate of the lower end of the crack is the largest, and the upper end of the crack is the smallest. When the loading span to radius ratio (S/R) is 0.6, the growth rate of the crack tip is the fastest.

Acknowledgement

There has been no significant financial support for this work that could have influenced its outcome.

References

[1] Kuruppu, M. D., Chong, K. P. "Fracture toughness testing of brittle materials using semi-circular bend (SCB) specimen", Engineering Fracture Mechanics, 91, pp. 133–150, 2012. https://doi.org/10.1016/j.engfracmech.2012.01.013

[2] Chong, K. P., Kuruppu, M. D. "New specimen for fracture toughness determination for rock and other materials", International Journal of Fracture, 26, pp. R59–R62, 1984. https://doi.org/10.1007/BF01157555

[3] Chong, K. P., Kuruppu, M. D., Kuszmaul, J. S. "Fracture toughness determination of layered materials", Engineering Fracture Mechanics, 28(1), pp. 43–54, 1987. https://doi.org/10.1016/0013-7944(87)90118-4

[4] Chong, K. P., Kuruppu, M. D. "Mixed mode fracture analysis using new semi-circular specimens", Computers and Structures, 30(4), pp. 905–908, 1988. https://doi.org/10.1016/0045-7949(88)90125-3

[5] Chong, K. P., Kuruppu, M. D. "New specimens for mixed mode fracture investigations of geomaterials", Engineering Fracture Mechanics, 30(5), pp. 701–712, 1988. https://doi.org/10.1016/0013-7944(88)90160-9

[6] Lim, I. L., Johnston, I. W., Choi, S. K. "Assessment of mixed-mode fracture toughness testing methods for rock", International Journal of Rock Mechanics and Mining Sciences & Geomechanics Abstracts, 31(3), pp. 265–272, 1994. https://doi.org/10.1016/0148-9062(94)90471-5

[7] Lim, I. L., Johnston, I. W., Choi, S. K., Boland, J. N. "Fracture testing of a soft rock with semi-circular specimens under three-point bending. part 1—mode I", International Journal of Rock Mechanics & Mining Sciences & Geomechanics Abstracts, 31(3), pp. 185–197, 1994. https://doi.org/10.1016/0148-9062(94)90463-4

[8] Aliha, M. R. M., Behbahani, H., Fazaeli, H., Rezaifar, M. H. "Study of characteristic specification on mixed mode fracture toughness of asphalt mixtures", Construction and Building Materials, 54, pp. 623–635, 2014. https://doi.org/10.1016/j.conbuildmat.2013.12.097

[9] Aliha, M. R. M., Bahmani, A., Akhondi, S. "Mixed mode fracture toughness testing of pmma with different three-point bend type specimens", European Journal of Mechanics, 58, pp. 148–162, 2016. https://doi.org/10.1016/j.euromechsol.2016.01.012

[10] Huang, B., Shu, X., Zou, G. "Using notched semi circular bending fatigue test to characterize fracture resistance of asphalt mixtures", Engineering Fracture Mechanics, 109, pp. 78–88, 2013. https://doi.org/10.1016/j.engfracmech.2013.07.003

[11] Zhao, Y., Gong, S., Jiang, Y., Han, C. "Characteristics of tensile strength and fracture properties of coal based on semi-circular bending tests", Chinese Journal of Rock Mechanics & Engineering, 35(6), pp. 1256–1264, 2016. [in Chinese] https://doi.org/10.13722/j.cnki.jrme.2015.0649

[12] Jiang, C., Zhao, G.-F., Zhu, J., Zhao, Y.-X., Shen, L. "Investigation of dynamic crack coalescence using a gypsum-like 3d printing material", Rock Mechanics and Rock Engineering, 49, pp. 3983–3998, 2016. https://doi.org/10.1007/s00603-016-0967-3

[13] Feng, G., Kang, Y., Meng, T., Hu, Y., Li, X. "The influence of temperature on mode I fracture toughness and fracture characteristics of sandstone", Rock Mechanics and Rock Engineering, 50, pp. 2007–2019, 2017. https://doi.org/10.1007/s00603-017-1226-y

[14] Wang, W., Olson, J. E., Prodanović, M., Schultz, R. A. "Interaction between cemented natural fractures and hydraulic fractures assessed by experiments and numerical simulations", Journal of Petroleum Science and Engineering, 167, pp. 506–516, 2018. https://doi.org/10.1016/j.petrol.2018.03.095

[15] Fu, J., Sarfarazi, V., Haeri, H., Marji, M. F., Guo, M. "Mechanism of failure in the Semi-Circular Bend (SCB) specimen of gypsum-concrete with an edge notch", Structural Engineering and Mechanics, 81(1), pp. 81–91, 2022 https://doi.org/10.12989/SEM.2022.81.1.081

[16] Fu, J., Sarfarazi, V., Haeri, H., Naderi, K., Marji, M. F., Guo, M. "The comparison between NBD test results and SCB test results using experimental test and numerical simulation", Advances in Concrete Construction, 13(1), pp. 83–99, 2022. https://doi.org/10.12989/ACC.2022.13.1.083

[17] Lim, I. L., Johnston, I. W., Choi, S. K. "Stress intensity factors for semi-circular specimens under three-point bending", Engineering Fracture Mechanics, 44(3), pp. 363–382, 1993. https://doi.org/10.1016/0013-7944(93)90030-V

[18] Zhao, G. F., Kazerani, T., Man, K., Gao, M., Zhao, J. "Numerical study of the semi-circular bend dynamic fracture toughness test using discrete element models", Science China Technological Sciences, 58, pp. 1587–1595, 2015. https://doi.org/10.1007/s11431-015-5887-z

[19] Eftekhari, M., Baghbanan, A., Hashemolhosseini, H. "Fracture propagation in a cracked semicircular bend specimen under mixed mode loading using extended finite element method", Arabian Journal of Geosciences, 8, pp. 9635–9646, 2015. https://doi.org/10.1007/s12517-015-1906-4

[20] Fayed, A. S. "Numerical evaluation of mode I/II SIF of quasi-brittle materials using cracked semi-circular bend specimen", Engineering Solid Mechanics, 6(2), pp. 175–186, 2018. https://doi.org/10.5267/j.esm.2018.1.002

[21] Haeri, H., Sarfarazi, V., Zhu, Z., Marji, M. F. "The effect of particle size on the edge notched disk (end) using particle flow code in three dimension", Smart Structures and Systems, 22(6), pp. 663–673, 2018. https://doi.org/10.12989/sss.2018.22.6.663

[22] Haeri, H., Sarfarazi, V., Zhu, Z., Moradizadeh, M. "The effect of ball size on the hollow center cracked disc (hccd) in brazilian test", Computers and Concrete, 22(4), pp. 373–381, 2018. https://doi.org/10.12989/cac.2018.22.4.373

[23] Fu, J.-W., Chen, K., Zhu, W., Zhang, X., Li, X. "Progressive failure of new modelling material with a single internal crack under biaxial compression and the 3-d numerical simulation", Engineering Fracture Mechanics, 165, pp. 140–152, 2016. https://doi.org/10.1016/j.engfracmech.2016.08.002

[24] Walters, M. C., Paulino, G. H., Dodds Jr., R. H. "Interaction integral procedures for 3-d curved cracks including surface tractions", Engineering Fracture Mechanics, 72(11), pp. 1635–1663, 2005. https://doi.org/10.1016/j.engfracmech.2005.01.002

[25] Li, F. Z., Shih, C. F., Needleman, A. "A comparison of methods for calculating energy release rates", Engineering Fracture Mechanics, 21(2), pp. 405–421, 1985. https://doi.org/10.1016/0013-7944(85)90029-3

[26] Williams, M. L. "On the stress distribution at the base of a stationary crack", Journal of Applied Mechanics, 24(1), pp. 109–114, 1956. https://doi.org/10.1115/1.4011454

[27] Toshio, N., Parks, D. M. "Determination of elastic t-stress along 3-d crack fronts using an interaction integral", International Journal of Solids and Structures, 29(13), pp. 1597–1611, 1992. https://doi.org/10.1016/0020-7683(92)90011-H

[28] Zhao, L. G., Tong, J., Byrne, J. "Stress intensity factor k and the elastic t-stress for corner cracks", International Journal of Fracture, 109, pp. 209–225, 2001. https://doi.org/10.1023/A:1011016720630

[29] Li, S., Yang, L., Li, M., Zhang, N. "Influences of 3d internal crack dip angle on tensile mechanical properties and fracture features of rock-like material", Chinese Journal of Rock Mechanics & Engineering, 28(2), pp. 281–289, 2009. [in Chinese]

[30] Tong, J. "T-stress and its implications for crack growth", Engineering Fracture Mechanics, 69(12), pp. 1325–1337, 2002. https://doi.org/10.1016/S0013-7944(02)00002-4

[31] Cotterell, B., Rice, J. R. "Slightly curved or kinked cracks", International Journal of Fracture, 16, pp. 155–169, 1980. https://doi.org/10.1007/BF00012619

[32] Fernandes, R., El-Borgi, S., Ahmed, K., Friswell, M. I., Jamia, N. "Static fracture and modal analysis simulation of a gas turbine compressor blade and bladed disk system", Advanced Modeling and Simulation in Engineering Sciences, 3, 30, 2016. https://doi.org/10.1186/s40323-016-0083-7